Thyroid deficiency before birth modifies adipose transcriptome to promote white adipose tissue growth and impair thermogenic capacity

Harris SE1, De Blasio MJ2, Zhao X2, Ma M3, Davies KL2, Wooding FBP2, Hamilton R2, Blache D4, Meredith D1, Murray AJ2, Fowden AL2 and Forhead AJ1,2

1Department of Biological and Medical Sciences, Oxford Brookes University, Oxford, OX3 0BP, UK; 2Department of Physiology, Development and Neuroscience, University of Cambridge, Cambridge, CB2 3EG, UK; 3Genomics-Transcriptomics Core, Wellcome Trust-MRC Institute of Metabolic Science, University of Cambridge, Cambridge, CB2 0QQ, UK; 4School of Animal Biology, University of Western Australia, 6009 Crawley, Australia

Submitted to Proceedings of the National Academy of Sciences of the United States of America

Development of adipose tissue before birth is essential for energy storage and thermoregulation in the neonate and for cardiometabolic health in later life. Thyroid hormones are important regulators of fetal growth and maturation. Offspring hypothyroid in utero are poorly adapted to regulate body temperature at birth and are at risk of becoming obese and insulin resistant in childhood. The mechanisms by which thyroid hormones regulate the growth and development of adipose tissue in the fetus, however, are unclear. The effect of thyroid deficiency (TX) on perirenal adipose tissue (PAT) development was examined in a fetal sheep model during late gestation. Hypothyroidism in utero resulted in elevated plasma insulin and leptin concentrations and overgrowth of PAT, specifically due to hyperplasia and hypertrophy of unilocular adipocytes with no change in multilocular adipocyte mass. RNA-sequencing and genomic analyses showed that TX affected 9-10% of the genes identified in fetal adipose tissue. Enriched KEGG and gene ontology pathways were associated with adipogenic, metabolic and thermoregulatory processes, insulin resistance, and a range of endocrine and adipocytokine signalling pathways. Adipose protein levels of signalling molecules, including S6-kinase, glucose transporter-4 and peroxisome proliferator-activated receptor-γ (PPARγ), were increased and uncoupling protein-1 (UCP1) were decreased by fetal hypothyroidism. Development of adipose tissue before birth, therefore, is sensitive to thyroid hormone status in utero. Changes to the adipose transcriptome and phenotype observed in the hypothyroid fetus may have consequences for the risk of obesity and metabolic dysfunction in later life.

fetus | thyroid hormones | adipose | insulin | leptin

Introduction

Development of adipose tissue before birth is crucial for energy storage, insulation and thermogenesis in the neonatal period and for cardiometabolic health in later life. In the fetus, adipose tissue comprises a mixture of both white and brown adipocyte types (1). White adipocytes, termed unilocular (UL), contain a large single lipid droplet and secrete a variety of adipokines, such as leptin, while brown adipocytes, termed multilocular (ML), are characterised by the presence of several smaller lipid droplets and an abundance of mitochondria with the capacity for non-shivering thermogenesis. Thermogenesis in ML adipocytes is enabled by the unique expression of uncoupling protein 1 (UCP1) on the inner mitochondrial membrane which uncouples the electron transport chain to generate heat.

The sheep fetus is commonly used to study adipose tissue development before birth. In human and ovine fetuses, adipose tissue first appears around mid-gestation with a major depot is located around the kidneys in both species (perirenal adipose tissue, PAT; 2). Towards term, changes in the structure and function of fetal adipose tissue are observed in the preparation for the nutritional and thermoregulatory challenges at birth (1). Differential gene expression profiles have been reported in ovine PAT perinatally as the structure of adipose tissue undergoes the transition from predominantly ML adipocytes at birth to UL adipocyte types at two weeks of postnatal life (1, 3). In fetal sheep, leptin and UCP1 mRNA abundances in PAT increase near term, in association with rising concentrations of cortisol and triiodothyronine (T3) in the circulation (4, 5).

Thyroid hormones, thyroxine (T4) and T3, have important roles in the control of growth, metabolism and development of the fetus (6). In animal models, experimental hypothyroidism *in utero* modifies fetal growth and impairs the maturation of organ systems, including the cardiovascular, nervous and skeletomuscular systems (6). Thyroid hormones are key regulators of neonatal body temperature, and hypothyroidism in fetal sheep impairs adipose thermogenic capacity and the ability to maintain body temperature at birth (7). Human neonates with congenital hypothyroidism (CH) are also at risk of developing hypothermia (8). Regulation of adipogenesis and adipose function by thyroid hormones during fetal life has important implications for the offspring, not only for survival in the immediate postnatal period but also for health in later life. Children and young adults diagnosed with CH at birth have an increased body mass index and are at greater risk of obesity, insulin resistance and non-alcoholic fatty liver, despite thyroid hormone treatment from diagnosis

Significance

Congenital hypothyroidism (CH) affects approximately 1 in 2000 neonates worldwide; affected infants are at risk of hypothermia and, even when treated soon after birth, are more likely to become overweight and insulin resistant in childhood. In a fetal sheep model, this study demonstrates that thyroid hormone deficiency in utero promotes unilocular-specific overgrowth of adipose tissue and adipocytokine secretion, in part via activation of insulin / insulin-like growth factor (IGF) and PPARγ signalling pathways. Fetal hypothyroidism impairs UCP1 thermogenic capacity without any change in multilocular adipocyte mass. These findings provide a mechanistic insight into the consequences of hypothyroidism before birth for the growth and development of adipose tissue, with important implications for neonatal survival and long term health.

Reserved for Publication Footnotes

Table 1. Mean (± SEM) plasma hormone concentrations, body and perirenal adipose tissue (PAT) weights, and adipose citrate synthase activity in sham and TX sheep fetuses at 129 and 143 days of gestation (dGA). * Significantly different from sham fetuses at the same gestational age; + significantly different from fetuses in the same treatment group at 129dGA; two-way ANOVA, P<0.05. ND, not detectable (minimum levels of detection: T4 7.0 ng/ml, T3 0.14 ng/ml).

	129 dGA		143 dGA	
	Sham (n=9)	TX (n=9)	Sham (n=10)	TX (n=10)
T4 (ng/ml)	81.1 ± 15.6	ND	82.9 ± 16.8	ND
T3 (ng/ml)	0.28 ± 0.07	ND	0.65 ± 0.13+	ND
Insulin (ng/ml)	0.30 ± 0.04	1.29 ± 0.31*	0.56 ± 0.12	1.68 ± 0.19*
Leptin (ng/ml)	0.52 ± 0.03	0.98 ± 0.06*	0.67 ± 0.05	1.05 ± 0.08*
Cortisol (ng/ml)	12.6 ± 3.1	9.8 ± 1.5	54.9 ± 12.7+	28.7 ± 3.9+
IGF-I (ng/ml)	18.4 ± 1.2	21.2 ± 2.8	27.0 ± 5.7	25.3 ± 3.1
IGF-II (ng/ml)	102.8 ± 10.4	118.8 ± 5.5	105.3 ± 6.7	106.3 ± 3.8
Body weight (kg)	2.61 ± 0.19	2.49 ± 0.20	3.58 ± 0.23+	3.13 ± 0.13+
Absolute PAT weight (g)	9.89 ± 0.62	12.67 ± 1.44	10.91 ± 1.13	14.71 ± 1.08*
Relative PAT weight (g/kg)	3.92 ± 0.32	5.19 ± 0.52*	3.12 ± 0.31	4.76 ± 0.40*
PAT citrate synthase activity (μmol/min/mg protein)	0.62 ± 0.06	0.35 ± 0.03*	0.92 ± 0.09+	0.47 ± 0.04*

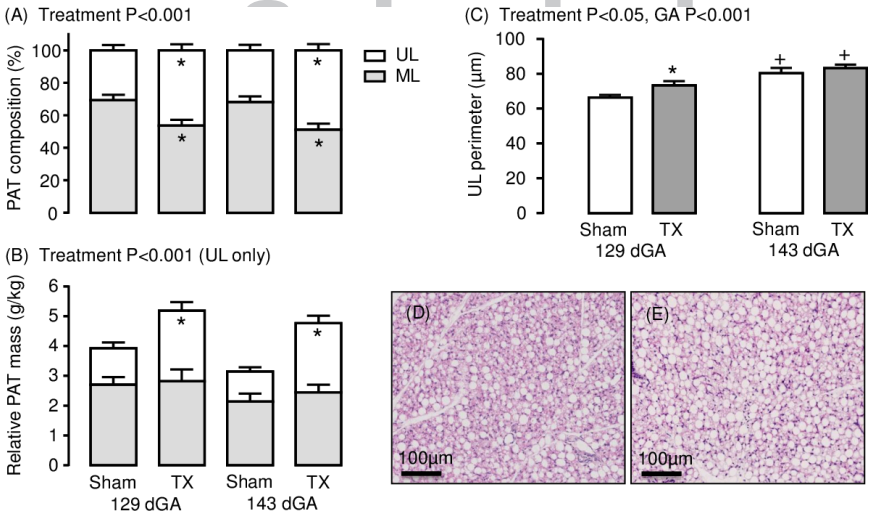

Fig. 1. Mean (± SEM) measurements of (A) perirenal adipose tissue (PAT) composition, (B) relative PAT mass and (C) unilocular (UL) adipocyte perimeter in sham and thyroidectomised (TX) fetuses at 129 and 143 days of gestation (dGA). * Significantly different from sham fetuses at same gestational age; + significantly different from fetuses at 129 dGA in the same treatment group, P<0.05. Representative histological images of perirenal adipose tissue taken from (D) sham and (E) TX sheep fetuses at 143 dGA. Haematoxylin and eosin stain.

(9-11). In rats, maternal hypothyroidism during pregnancy also increases visceral fat mass and causes glucose intolerance in the adult offspring, in association with tissue-specific changes in the expression of the glucose-transporters (GLUT) 1 and 4 (12, 13). Intrauterine programming of adiposity has implications for adult insulin sensitivity and cardiometabolic disease (14). Cross-talk between adipose tissue, especially PAT, liver and skeletal muscle may be mediated by adipose-derived factors such as free fatty acids and adipocytokines. In adult humans, PAT thickness has been correlated with increased risk of conditions including hypertension, fatty liver and coronary heart disease (15).

The aims of the current study were to determine the effects of hypothyroidism *in utero* on the growth and development of ovine adipose tissue, and to determine the molecular mechanisms responsible using transcriptome profiling. The study tested the hypothesis that thyroid hormone deficiency during late gestation would increase and decrease the amounts of UL and ML adipocytes, respectively, and impair the thermogenic capacity near term. The structure, transcriptome and protein expression was assessed in PAT from twin sheep fetuses, in which the thyroid gland of one twin was surgically removed during late gestation while the other was sham-operated as a control.

Results

Hypothyroidism *in utero* increases circulating insulin and leptin concentrations

In TX fetuses, plasma T4 and T3 concentrations decreased to below the limits of assay detection at both 129 and 143 dGA (Table 1). The normal developmental rise in plasma T3 concentration was observed in the sham fetuses (P<0.05; Table 1). Compared to the sham fetuses, TX fetuses had higher plasma concentrations of insulin and leptin at both gestational ages (P<0.05; Table 1). Plasma cortisol concentration was higher in both groups of fetuses studied at 143 dGA compared to those studied at 129 dGA (P<0.05; Table 1); fetal hypothyroidism tended to suppress plasma cortisol concentration (P=0.052). Plasma concentrations of IGFI and IGFII were unaffected by TX or gestational age (Table 1).

UL-specific adipocyte growth and proliferation enlarges adipose tissue mass in hypothyroid fetuses

In TX fetuses, absolute PAT weight was greater than in sham fetuses at 143, but not 129 dGA (P<0.05; Table 1); the PAT mass relative to body weight was higher in TX than sham fetuses at both ages (P<0.05, Table 1). When expressed as a percentage of total PAT volume, sham fetuses had a greater percentage of

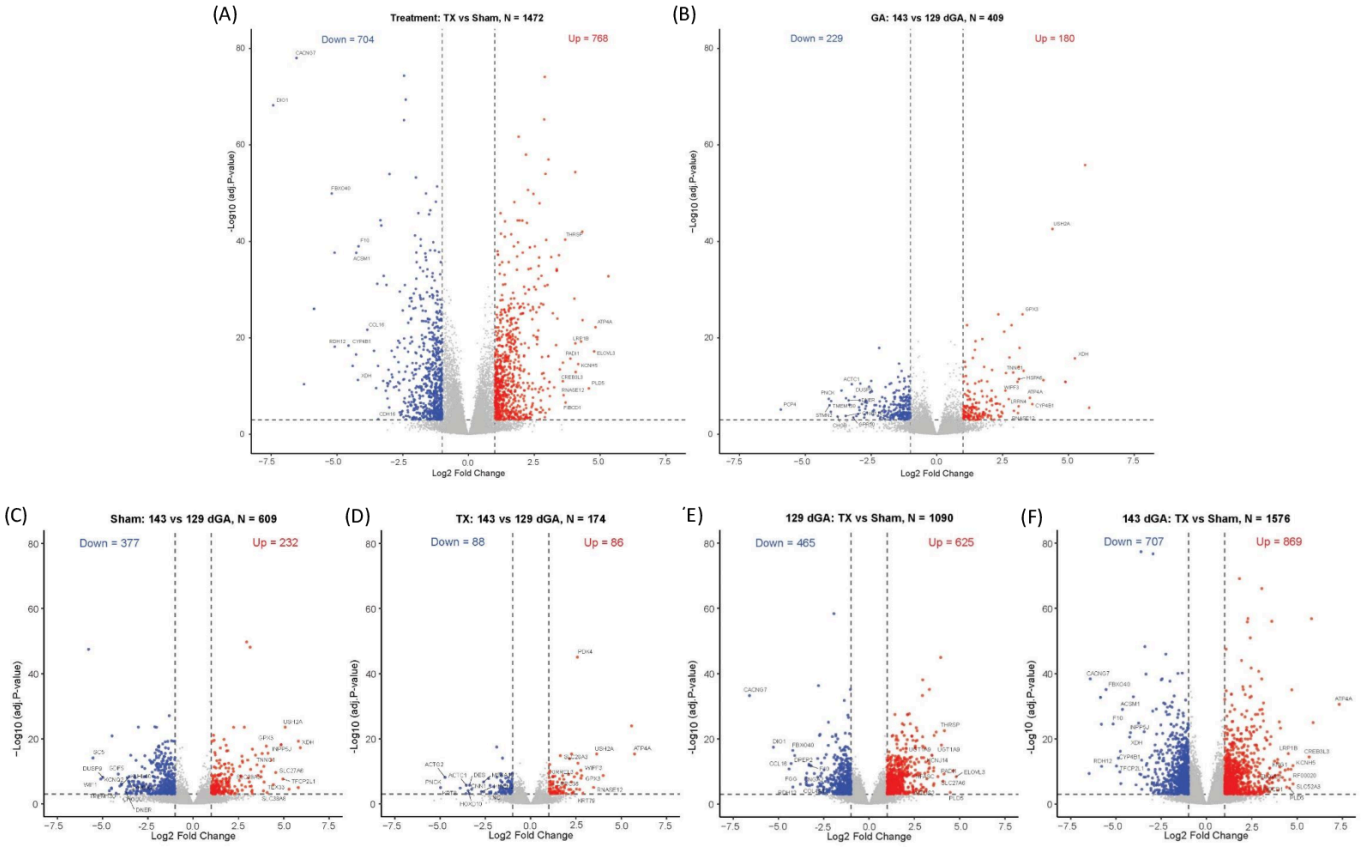

Fig. 2. Volcano plots using RNA-sequencing data from perirenal adipose tissue taken from sham and thyroidectomised (TX) fetuses at 129 and 143 days of gestation (dGA). Volcano plots comparing data by treatment (A: TX and sham) and gestational age (B: 129 and 143 dGA), and between and within treatment and gestational age groups (C-F). Red and blue dots represent up and down-regulated differentially expressed genes, respectively (absolute log2 fold change >= 1, Padj < 0.05). The top 10 genes are labelled for both up and down-regulated genes.

ML relative to UL adipocyte types at 129 and 143dGA ($P<0.001$, Figure 1A). In TX fetuses, there was an increase in the percentage of UL, and a decrease in ML, adipocytes compared to control values at both ages ($P<0.001$; Figure 1A). When the percentages of ML and UL adipocytes were expressed as absolute and relative masses, a 0.95-1.30-fold increase in UL adipocyte mass was observed in the TX fetuses at both 129 and 143dGA ($P<0.05$, Figure 1B). The absolute and relative ML adipocyte masses, and fetal body weight, were unaffected by TX (Table 1, Figure 1B). Positive correlations were observed between the relative UL adipocyte mass and fetal concentrations of insulin ($R=0.49$, $N=37$, $P<0.005$) and leptin ($R=0.68$, $N=38$, $P<0.001$). The average perimeter of the largest UL adipocytes increased with hypothyroidism ($P<0.05$) and gestational age ($P<0.001$; Figure 1C). These data suggest that the increase in PAT mass observed after TX was due to increased UL-specific adipocyte growth and proliferation (Figure 1D and E).

Adipose transcriptome analysis reveals differential gene expression profiles in response to hypothyroidism *in utero*

RNA-sequencing was undertaken on PAT samples from sham and TX fetuses at both 129 and 143 dGA and the distribution of gene expression was assessed initially by principal component analysis (PCA). Using the top 500 most variable genes, the PCA plot identified two distinct clusters of data based on treatment group and further sub-division by gestational age (Supplementary Figure 1A). The MA plot and heat map for the top 262 genes demonstrated differential gene expression profiles by treatment and gestational age (Supplementary Figure 1B and C)? In total, 16137 genes were identified in the adipose samples from the annotated sheep genome. When data from all animals were considered with an absolute log2 fold change of at least 1, a total of 1472 genes were affected by hypothyroidism (768 up and 704 down-regulated by TX; Figure 2A) and 409 were affected by increasing gestational age (180 up, 229 down with increased gestational age; Figure 2B). When the data were analysed by age in each treatment group, the expression of 609 genes changed between 129 and 143 dGA in the sham fetuses (232 up, 377 down; Figure 2C), while this number was reduced to 174 in the TX fetuses over the same time period (86 up, 88 down; Figure 2D). When the data were analysed by treatment at each age, TX influenced the expression of more genes at 143 dGA (1576 total, 869 up, 707 down; Figure 2F) than at 129 dGA (1090 total, 625 up, 465 down; Figure 2E). Supplementary Figure 2?

Gene ontology and KEGG pathway analyses identify adipogenic, metabolic, thermogenic and hormone signalling processes influenced by hypothyroidism *in utero*

A number of biological pathways were identified as enriched in PAT from TX fetuses. Of particular relevance, enriched KEGG pathways were associated with regulation of lipolysis; fatty acid synthesis and metabolism; insulin resistance; AMPK, FoxO and cAMP signalling; and signalling pathways for insulin, peroxisome proliferator-activated receptor (PPAR) and adipocytokines (Figure 3). Biological process pathways over-represented in the gene ontology analysis included fatty acid metabolism and biosynthesis, and several aspects of thermogenesis and temperature regulation (Figure 4). When the data were assessed by treatment and age, an additional number of enriched pathways were identified in TX fetuses at 129 dGA including apelin and thyroid hormone signalling pathways (Figure 3A) and lipid metabolism (Figure 4).

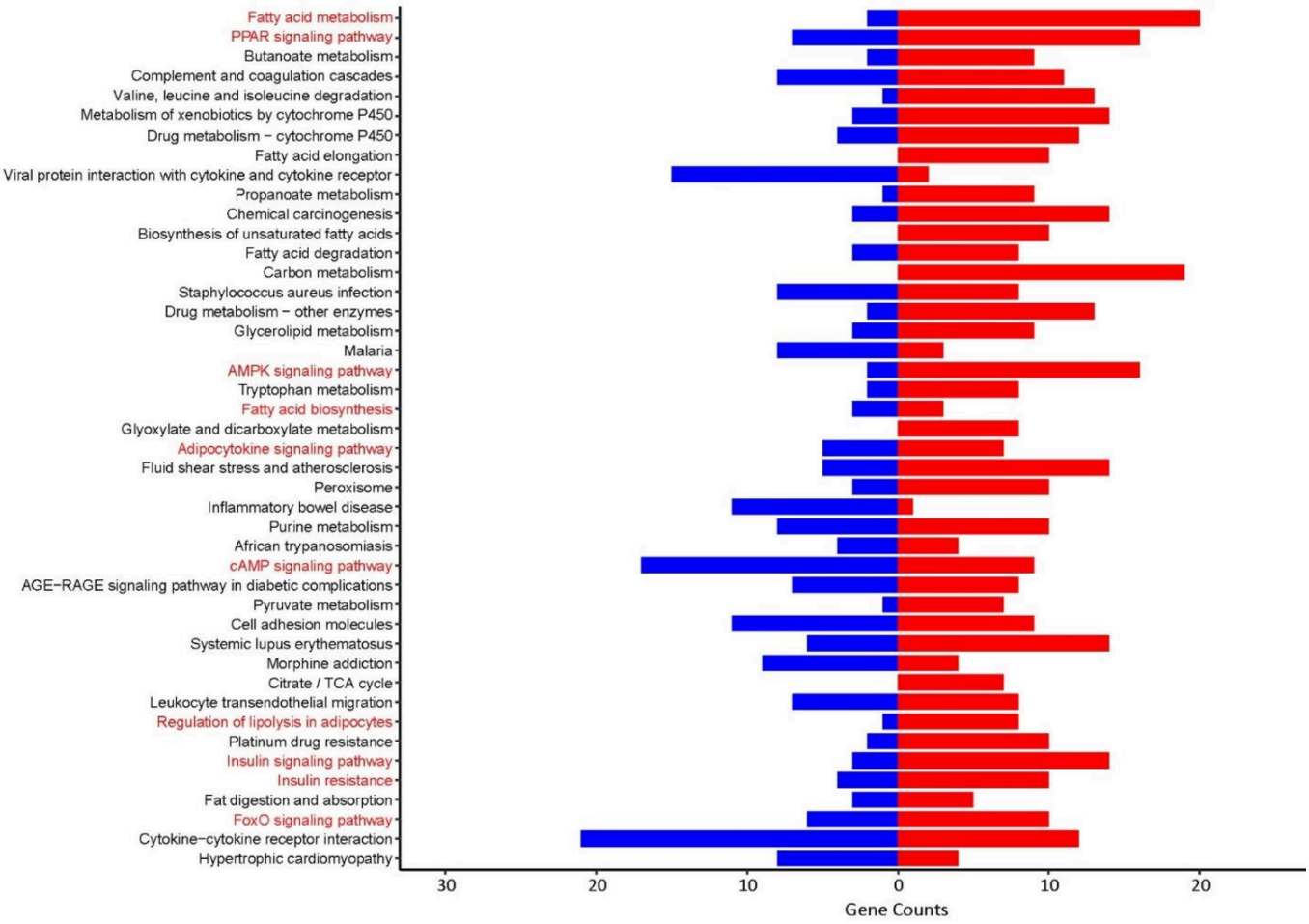

Fig. 3. KEGG pathway bar plot using RNA-sequencing data from perirenal adipose tissue taken from sham and thyroidectomised (TX) fetuses at 129 and 143 days of gestation (dGA). KEGG pathway bar plot indicating the number of up and down-regulated genes when the data were compared by treatment (TX and sham); the red and blue bars represent up and down-regulated genes, respectively.

Hypothyroidism *in utero* activates adipose PPAR and insulin-IGF signalling

Key genes in some of the enriched pathways were examined in more detail and protein content was quantified by Western blotting. Increased mRNA and protein contents of the mitotic marker, proliferating cell nuclear antigen (PCNA), and PPARγ, an important regulator of adipocyte differentiation, were observed in response to fetal hypothyroidism ($P<0.005$, Figure 5A and B). Adipose PCNA mRNA abundance decreased between 129 and 143 dGA in sham fetuses ($P<0.05$), and PCNA mRNA and protein contents were higher in TX compared sham fetuses at 143 dGA ($P<0.05$; Figure 5Ai and ii). Compared with control values, both the mRNA and protein contents of PPARγ at 129 dGA, and mRNA abundance at 143 dGA, were greater in TX fetuses ($P<0.05$; Figure 5Bi and ii). Adipose mRNA abundances of IGFI and IGFII and leptin were also increased by TX ($P<0.001$, Figure 6A, B and C). An increase in adipose IGFI mRNA was observed between 129 and 143 dGA in TX fetuses ($P<0.05$; Figure 6A); over the same period, IGFII mRNA abundance decreased in both sham and TX fetuses ($P<0.05$; Figure 6B).

To examine if hyperinsulinaemia and increased adipose IGF mRNA abundance observed in TX fetuses were responsible, at least in part, for the greater PAT mass, the expression of insulin-IGF and adipokine signalling pathways were investigated in sham and TX fetuses. At 129 dGA, the mRNA abundance of the insulin receptor was higher, while insulin receptor β-subunit (InsRβ) protein content was lower in TX fetuses compared to sham fetuses ($P<0.05$, Figure 5Ci and ii). Between 129 and 143 dGA, a reduction in InsRβ protein was seen in sham, but not TX fetuses ($P<0.05$, Figure 5Cii). At 129 dGA, protein kinase β 1 (Akt1) and Akt2 mRNA, and Akt1 protein content, were greater in TX compared to sham fetuses ($P<0.05$, Figure 5D-E). In the TX fetuses, Akt2 mRNA abundance decreased between 129 and 143 dGA, and Akt2 protein content was lower at 143 dGA compared to that observed in sham fetuses ($P<0.05$, Figure 5E). The total amount of phosphorylated Akt (pAkt) protein did not change with age or fetal hypothyroidism (data not shown).

A developmental rise in mRNA abundance of the mammalian target of rapamycin (mTOR) was observed in sham, but not TX fetuses ($P<0.05$, Figure 5Fi); at 143 dGA only, mTOR mRNA abundance was lower in TX than sham fetuses ($P<0.05$, Figure 5Fi). Fetal hypothyroidism reduced pmTOR protein content ($P<0.05$), although *post-hoc* analysis failed to identify significant differences at either age (Figure 5Fii). At 129 dGA, pS6 kinase (pS6K) protein content was higher in TX than sham fetuses ($P<0.05$), and decreased with increasing age in TX but not sham fetuses ($P<0.05$, Figure 5Gii); S6K mRNA abundance, however, was unaffected by fetal TX and age (Figure 5Gi). In TX fetuses, mRNA abundance of the insulin-sensitive glucose transporter, GLUT4, was greater than that observed in sham fetuses at 129 dGA and decreased towards term, unlike sham fetuses ($P<0.05$, Figure 5Hi). Adipose GLUT4 protein content was also greater in TX than sham fetuses at both ages ($P<0.05$, Figure 5Hii).

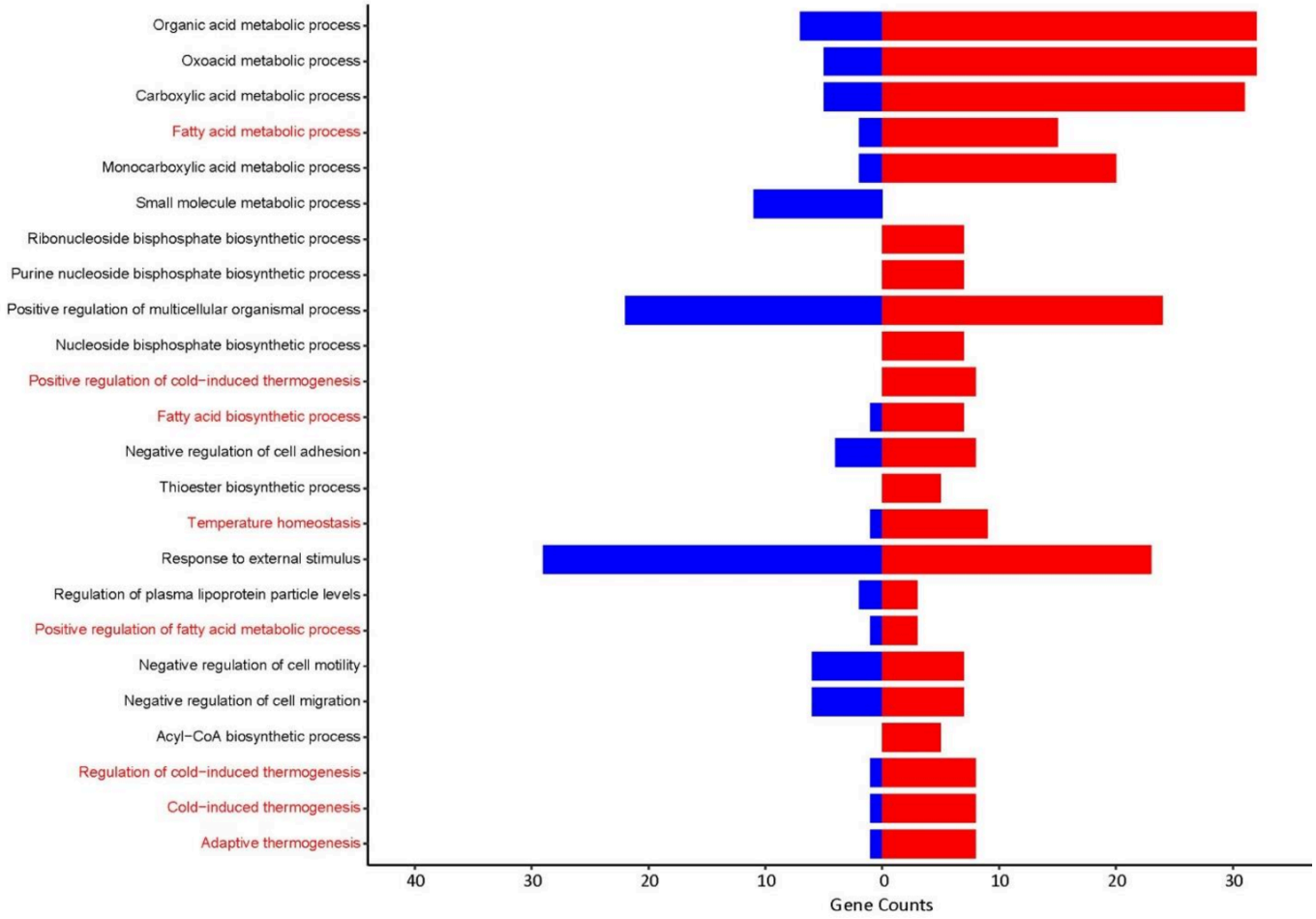

Fig. 4. Biological process (BP) ontology pathway bar plot using RNA-sequencing data from perirenal adipose tissue taken from sham and thyroidectomised (TX) fetuses at 129 and 143 days of gestation (dGA). BP ontology pathway bar plot indicating the number of up and down-regulated genes when the data were compared by treatment (TX and sham); the red and blue bars represent up and down-regulated genes, respectively.

Developmental increments in adipose adrenergic receptor (ADR) α1A mRNA abundance were observed between 129 and 143 dGA in both sham and TX fetuses, without any effect of TX ($P<0.05$, Figure 6D). Adipose ADRβ2 mRNA abundance also increased towards term in sham but not TX fetuses; ADRβ2 mRNA abundance was lower in TX compared to sham fetuses at 143 DGA ($P<0.05$, Figure 6H). At 129 dGA, the mRNA abundance of ADRα1D was lower, while that of ADRβ1 and ADRβ3 were all higher, in TX than sham fetuses ($P<0.05$, Figure 6E, G and I). Adipose ADRα2A was increased by TX at both 129 and 143 dGA ($P<0.05$, Figure 6F). There were no effects of TX or age on the amount of the long-form leptin receptor protein, ADRα1B mRNA abundance, or the mRNA or protein abundance of the IGF type 1 receptor in PAT (data not shown).

Hypothyroidism *in utero* impairs adipose thermogenic capacity

Although the absolute and relative masses of ML adipocytes were unaffected by TX, the capacity for non-shivering thermogenesis was impaired in the PAT of TX fetuses. Adipose citrate synthase (CS) activity, as a proxy measure of mitochondrial number, increased between 129 and 143 dGA in sham but not TX fetuses ($P<0.05$, Table 1); CS activity in the TX fetuses was lower than control values at both ages ($P<0.05$, Table 1). Both adipose UCP1 mRNA and protein content (both absolute value and when expressed relative to CS activity) increased near term in sham fetuses, but these developmental changes were abolished by TX (Figure 5Ii and ii). Adipose UCP1 mRNA abundance was lower in TX compared to sham fetuses at 143 dGA ($P<0.05$, Figure 5Ii); UCP1 protein content was reduced by TX at both 129 and 143 dGA ($P<0.05$, Figure 5Iii) in line with previous findings at term (7).

Hypothyroidism *in utero* alters adipose thyroid hormone metabolism and signalling

Adaptive changes in adipose mRNA abundance for the iodothyronine deiodinases (DIO) and thyroid hormone receptors (TR) were observed in response to TX. Towards term, significant increments in the mRNA abundance of DIO1 and DIO2 were observed in sham but not TX fetuses ($P<0.05$, Figure 7A and B). In TX fetuses, lower mRNA levels were observed for DIO1 at 143 dGA, and DIO2 at 129 dGA, compared to the sham fetuses ($P<0.05$, Figure 7A and B). Adipose mRNA levels of TRα and TRβ were increased by TX at both ages ($P<0.05$, Figure 7C and D); a significant increase in adipose TRβ mRNA was observed in sham fetuses near term ($P<0.05$, Figure 7D).

Discussion

This study has shown for the first time that thyroid hormone deficiency modifies the growth and development of fetal adipose tissue, in manner that is likely to compromise the ability of the neonate to maintain body temperature at birth and to increase its risk of cardiometabolic dysfunction in later life. Fetal hypothyroidism caused a shift in the relative composition of UL and ML adipocyte types towards an increase in UL adipocyte mass due to hyperplasia and hypertrophy. Markers of UL adipocyte type,

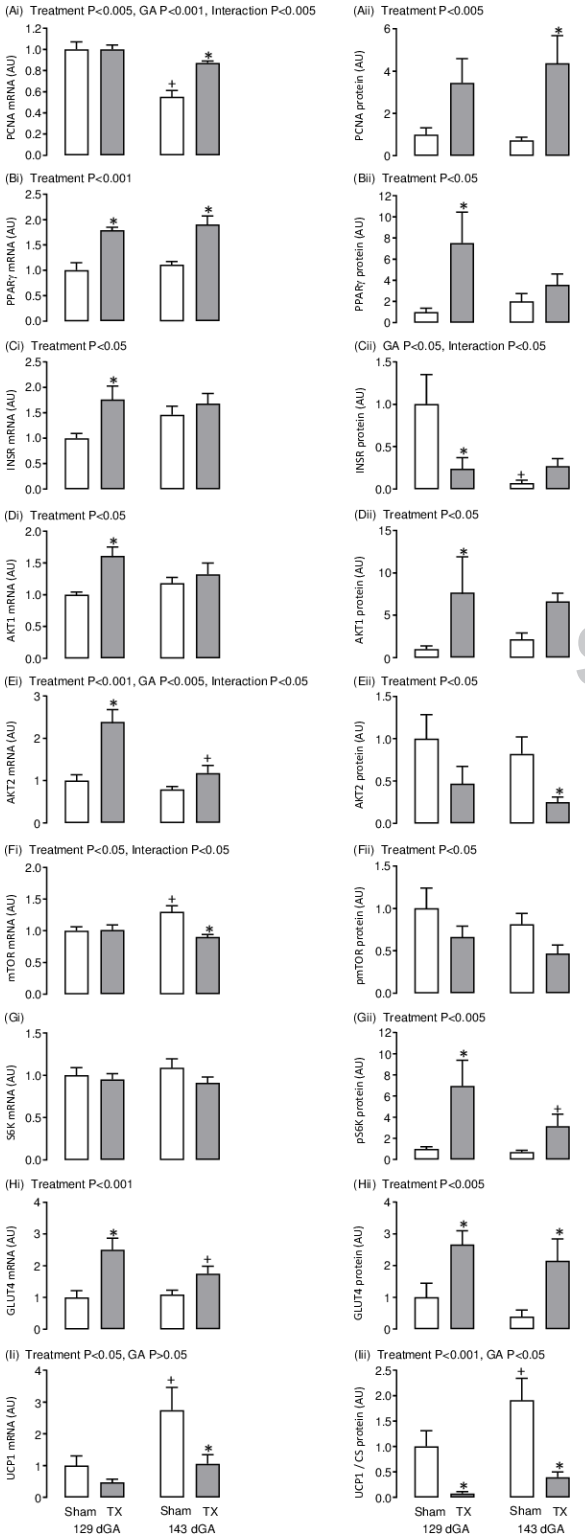

Fig. 5. Mean (± SEM) mRNA abundance of (A) insulin-like growth factor-I (IGFI), (B) IGFII, (C) leptin and the adrenergic receptors (D) α1A, (E) α1D, (F) α2A, (G) β1, (H) β2 and (I) β3 in perirenal adipose tissue taken from sham and thyroidectomised (TX) fetuses at 129 and 143 days of gestation (dGA). * Significantly different from sham fetuses at same gestational age; + significantly different from fetuses at 129 dGA in the same treatment group, P<0.05. AU, arbitrary units.

such as leptin, adiponectin and lipoprotein lipase, were increased in TX ovine fetuses, and adipocyte proliferation was indicated by elevated levels of the mitotic marker PCNA and enrichment of gene pathways responsible for PPARγ and insulin-IGF signalling. The percentage of ML adipocytes in PAT was reduced by hypothyroidism *in utero* and, although the total amount of ML adipose tissue did not differ between sham and TX fetuses, UCP1 expression and thermogenic capacity were impaired relative to mitochondrial number indicated by CS activity. Furthermore, bioinformatic analysis showed that, for a substantial number of genes, hypothyroidism prevented the maturational changes normally seen in the transcriptome of ovine PAT near term.

The effects of thyroid hormone deficiency before birth may be direct, via thyroid hormone response elements on target genes (16), and/or indirect, via interactions with other nuclear receptors or changes in fetal hormone concentrations. The increased circulating concentration of insulin seen in the hypothyroid sheep fetus, secondary to pancreatic B-cell proliferation (17), may be responsible, at least in part, for UL-specific PAT overgrowth. Indeed, a positive correlation was observed between fetal insulin concentration and relative UL adipocyte mass in the present study. Before birth, insulin stimulates growth of the axial skeleton and tissues such as adipose tissue (18). In the ovine fetus, hyperglycaemia and hyperinsulinaemia induced by fetal glucose infusion has also been shown to promote UL adipocyte growth with no change in ML adipocyte mass (19). A variety of signalling pathways responsive to insulin and the IGFs, and known to be involved in the control of adipogenesis, were enriched in the adipose transcriptome (including PPARγ, apelin, FoxO signalling) by hypothyroidism *in utero*. Furthermore, measurement of selected downstream target proteins showed upregulation of pS6K, GLUT4 and PPARγ in TX fetuses. Phosphorylation of S6K, without any change in mRNA abundance, indicated activation of the PI3-kinase pathway which is known to regulate adipogenesis via a range of transcription factors and interacting molecular pathways (20, 21). Transgenic mice with mutation in the S6K gene are growth retarded from embryonic life with reductions in pancreatic β-cell size and insulin content (22). This phenotype persists to adulthood and is associated with impaired adipogenesis, increased insulin sensitivity and resistance to diet-induced obesity (23). Increased adipose GLUT4 mRNA abundance and protein expression in TX sheep fetuses may also contribute to adipogenesis via enhanced glucose uptake and lipid storage, and are consistent with findings in rat pups hypothyroid in fetal and neonatal life (24).

While circulating IGF levels remained unchanged in TX sheep fetuses, adipose mRNA abundances for IGFI and II were elevated, indicating potential upregulation of local synthesis and paracrine actions of the IGFs. Thyroid hormone deficiency *in utero* has been shown previously to modify IGF expression in liver and skeletal muscle with tissue-specific effects on growth and development in fetal sheep (25, 26). Insulin-IGF signalling pathways can also induce the synthesis of adipokines, such as leptin, apelin and adiponectin, in part via interactions with PPARγ signalling. Previous studies have shown that hyperinsulinaemia, in the presence of euglycaemia, increases adipose leptin mRNA abundance in fetal sheep (27). High circulating levels of thyroid-stimulating hormone associated with TX may also stimulate leptin secretion, as reported in human adipose tissue cultured *in vitro* (28). The extent to which the increase in adipose adipokine expression and circulating leptin levels in the hypothyroid sheep fetus result from the greater UL adipocyte mass and/or greater capacity for adipokine synthesis and secretion in individual UL adipocytes remains to be established.

Hypothyroidism *in utero* did not affect the total mass of ML adipocytes in fetal sheep, but the thermogenic capacity of PAT, indicated by UCP1 expression, was impaired. The mRNA and protein abundances of UCP1 were reduced and several genes in the thermogenic pathways were affected by thyroid hormone

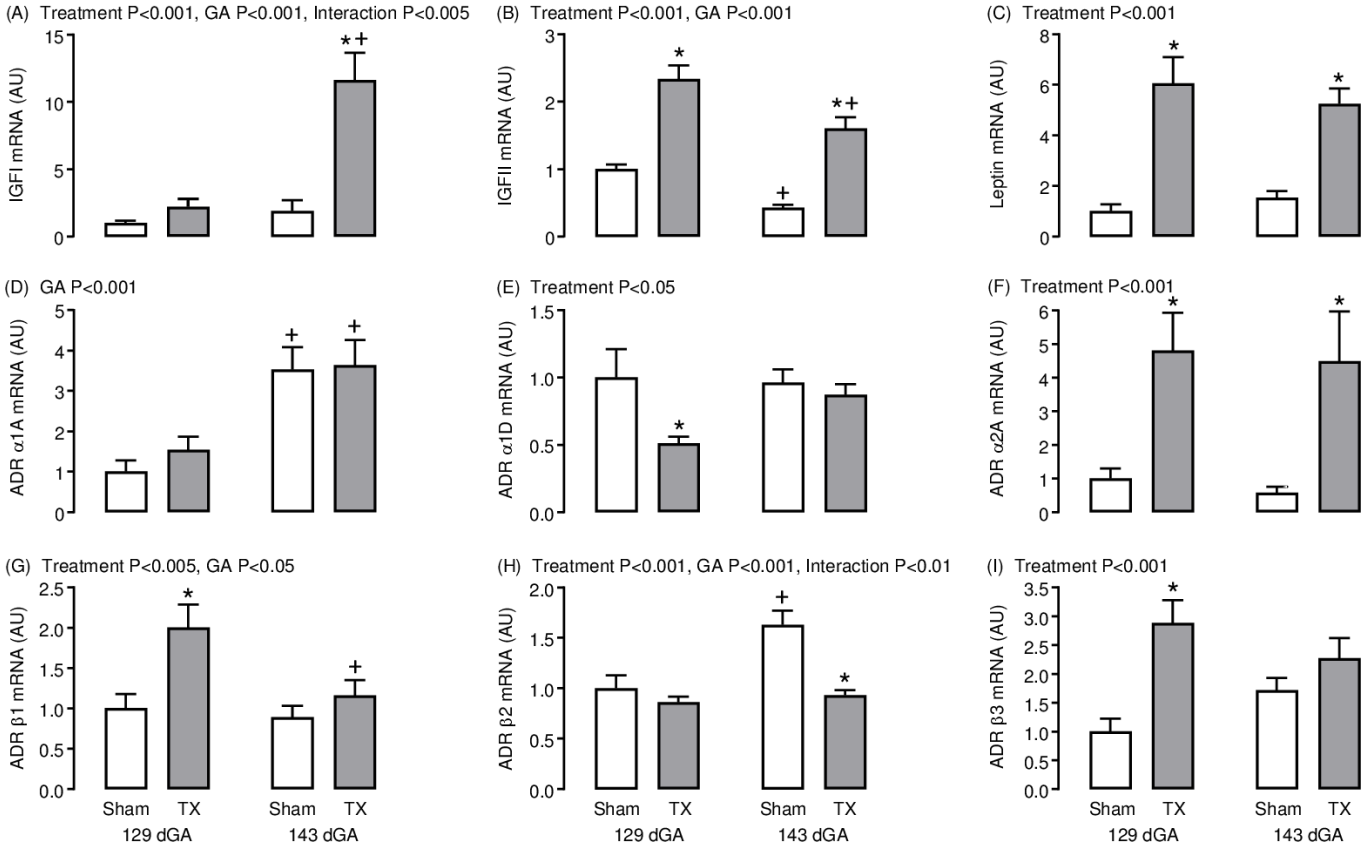

Fig. 6. Mean (± SEM) mRNA and protein abundance of (Ai, ii) proliferating cell nuclear antigen (PCNA), (Bi, ii) peroxisome proliferator-activated receptor γ (PPARγ), (Ci, ii) insulin receptor (INSR), (Di, ii) protein kinase β 1 (Akt1), (Ei, ii) Akt2, (Fi, ii) mammalian target of rapamycin (mTOR, phosphorylated protein), (Gi, ii) S6 kinase (S6K, phosphorylated protein), (Hi, ii) glucose transporter-4 (GLUT4), and (Ii, ii) uncoupling protein-1 (UCP1), where UCP1 protein content was expressed relative to citrate synthase (CS) activity, in perirenal adipose tissue taken from sham and thyroidectomised (TX) fetuses at 129 and 143 days of gestation (dGA). * Significantly different from sham fetuses at same gestational age; + significantly different from fetuses at 129 dGA in the same treatment group, P<0.05. AU, arbitrary units.

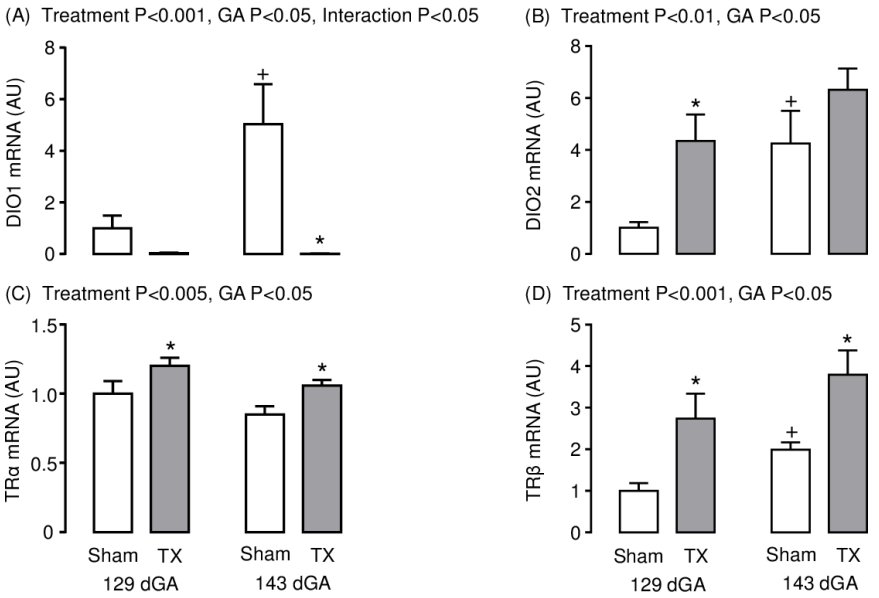

Fig. 7. Mean (± SEM) mRNA abundance of (A) iodothyronine deiodinase-1 (DIO1), (B) DIO2, (C) thyroid hormone receptor α (TRα) and (D) TRβ in perirenal adipose tissue taken from sham and thyroidectomised (TX) fetuses at 129 and 143 days of gestation (dGA). * Significantly different from sham fetuses at same gestational age; + significantly different from fetuses at 129 dGA in the same treatment group, P<0.05. AU, arbitrary units.

deficiency. Previous studies have shown that hypothyroid lambs are unable to maintain normal body temperature at delivery and their PAT contains less UCP1 and more lipid (7). Maternal hypothyroidism in rats led to low adipose UCP1 mRNA abundance in the fetuses which correlated with adipose T3 levels and was corrected by maternal thyroid hormone treatment (29). Furthermore, in cultured brown adipocytes taken from fetal rats, T3 causes an increase in UCP1 gene transcription, mRNA stability

and mitochondrial protein content (30). Moreover, a thyroid hormone response element (TRE) has been reported upstream of the promoter region of the UCP1 gene (31). Suppression of adipose UCP1 levels were observed in TX sheep fetuses despite upregulation of other factors known to stimulate UCP1 expression, such as ADRβ3, IGFI, leptin and PPARγ, possibly as compensatory mechanisms. The sympathomedullary system is primarily activated at birth by delivery into a cold environment and normally interacts with thyroid hormones to promote UCP1 expression and non-shivering thermogenesis. Although plasma catecholamines concentrations were not measured in the present study, PAT catecholamine content has been reported unaffected by TX in fetal sheep (32). Previous studies have also shown that noradrenergic-induced cellular respiration in PAT is suppressed in TX sheep fetuses, compared with those infused with T3, which suggests that functional adrenergic signalling may be impaired, despite elevated PAT mRNA abundance of some ADR isoforms (33).

Maturational changes in thyroid hormone metabolism and signalling were observed in fetal adipose tissue during late gestation, which were modified by thyroid hormone deficiency. In sham fetuses, mRNA abundances of iodothyronine deiodinases DIO1 and DIO2 (which both metabolise T4 to the biologically active T3), and the thyroid hormone receptor TRβ, increased towards term. Upregulation of DIO1 and DIO2 enzyme activities have been demonstrated previously in ovine fetal PAT over the same period of gestation, in part due to the prepartum rise in plasma cortisol (34, 35). Increased DIO1 enzyme activity in the PAT, and liver and kidney, of the sheep fetus near term are likely to be responsible for the increase in plasma T3 seen close to term (35). Hypothyroidism *in utero* had contrasting effects on the expression of DIO1 and DIO2 mRNA in ovine fetal PAT: DIO1 was reduced to negligible levels and DIO2 was increased in TX fetuses, in line with previous findings on deiodinase enzyme activity in adipose and other tissues of hypothyroid sheep and rat fetuses (29, 34, 36). Indeed, bioinformatic analysis identified DIO1 as the top-ranked gene affected by fetal TX in the current study with a 7.4-fold decrease in expression levels. Although DIO2 enzyme activity is much lower than DIO1 in ovine fetal PAT (35), the increase in DIO2 mRNA abundance may be an adaptive response to maintain local T3 production in hypothyroid conditions. The molecular mechanisms responsible for the tissue-specific control of deiodinase expression by thyroid hormone deficiency before birth remain to be established, although a TRE has been identified in the human Dio1 gene (37). Within the PAT of TX sheep fetuses, the mRNA abundances of both thyroid hormone receptors, TRα and β, were increased in an attempt to maintain local sensitivity to thyroid hormones in the face of systemic hypothyroidism.

During hypothyroidism *in utero*, activation of adipogenesis, suppression of thermogenic capacity, and exposure of the fetus to high circulating levels of insulin and adipocytokines may have consequences for adipose function and insulin sensitivity in the longer term (14). Human infants exposed to hyperinsulinaemia before birth, such as those born to obese mothers, have greater percentage body fat, umbilical cord leptin concentration and indicators of insulin resistance compared to those born to lean mothers (38). In the present study, genomic pathways associated with insulin resistance were identified as enriched in PAT from TX fetuses. Furthermore, since there is a link between adiposity in the neonate and child (39), these findings suggest that the development of fetal adipose tissue and enhancement of insulin resistance pathways may predispose offspring hypothyroid *in utero* to obesity and metabolic disease in later life. Indeed, several studies worldwide have shown that children born with CH have a greater body mass index and are more at risk of obesity, insulin resistance and NAFL in early and young adult life compared with the general population, even when diagnosed and treated with T4 soon after birth (9-11, 40, 41). Moreover, infants with more moderate reductions in thyroid hormones associated with prematurity or intrauterine growth retardation are also at greater risk of obesity and cardiometabolic dysfunction in later life (6, 14). Collectively, these findings suggest that exposure to hypothyroidism *in utero* permanently alters adipose tissue development with consequences for adult health. Further investigations are required, however, to determine whether these programming effects arise directly from the altered adipose phenotype and/or indirectly from other changes in endocrine activity, metabolism or appetite regulation that affect adult adiposity. For example, antithyroid drug treatment in pregnant rats leads to hyperleptinaemia in the adult offspring and alterations in hypothalamic leptin signalling molecules indicative of leptin resistance (42). Hyperinsulinaemia and overgrowth of UL adipose tissue in sheep fetuses infused with glucose were also associated with changes to the expression of neuropeptides in the appetite-regulatory regions of the hypothalamus (19).

In summary, hypothyroidism before birth caused an increase in PAT mass which was due to UL-specific adipocyte growth and proliferation. Greater deposition of UL adipocyte mass in the TX fetus was associated with increased circulating concentrations of insulin and leptin, and increased mRNA and protein expression of insulin-IGF and PPARγ signalling pathways. The adipose molecular pathways affected by thyroid hormone deficiency *in utero* indicate impaired thermogenic capacity and insulin resistance and may have consequences for neonatal survival and metabolic health in adulthood.

Materials and Methods

Animals

All surgical and experimental procedures were carried out in accordance with UK Home Office legislation and the Animals (Scientific Procedures) Act 1986, after ethical approval by the University of Cambridge Animal Welfare and Ethical Review Body at the Department of Physiology, Development and Neuroscience, University of Cambridge, UK. Nineteen Welsh Mountain pregnant ewes of known gestational age and carrying twin fetuses (15 female and 23 male) were used in this study. The ewes were housed in individual pens and were maintained on 200 g/day concentrates with hay and water *ad libitum* and access to a salt block. Food, but not water, was withheld from the ewes for 18-24 hours before surgery.

Experimental procedures

At 105-110 days of gestation (dGA; term ~ 145 ± 2 days) and under halothane anaesthesia (1.5 % halothane in O_2-N_2O), the twin fetuses of each ewe underwent either a thyroidectomy (TX) or a sham operation in which the thyroid gland was exposed but not removed (sham), as described previously (43). At either 129 (n=18) or 143 dGA (n=20), the fetuses were delivered by Caesarean section under general anaesthesia (20 mg/kg maternal body weight sodium pentobarbitone I.V.). Blood samples were collected by venepuncture of the umbilical artery into EDTA-containing tubes. Each fetus was weighed and a variety of fetal organs, including the PAT, were collected after the administration of a lethal dose of barbiturate (200 mg/kg sodium pentobarbitone iv).

Plasma hormone measurements

Umbilical plasma T3 and T4 concentrations were determined by RIA (MP Biomedicals, Loughborough, UK); the intra-assay coefficients of variation were 3 % and 5 %, and the minimum levels of detection were 0.14 and 7.0 ng/ml, respectively. Plasma insulin and cortisol concentrations were determined using ELISA kits (insulin: Mercodia, Uppsala, Sweden; cortisol: IBL International, Hamburg, Germany); the intra-assay coefficients of variation were both 9%, and the minimum levels of detection were 0.025 and 2.5 ng/ml, respectively. Plasma concentrations of leptin, IGF-I and IGF-II were determined by RIA as previously described (44, 45). The intra-assay coefficients of variation were 4-5 %, and the minimum levels of detection were 0.09, 0.08 and 4.0 ng/ml, respectively.

Adipose tissue histology

Fetal PAT was fixed in 4 % paraformaldehyde (with 0.2 % glutaraldehyde in 0.1 M phosphate buffer, pH 7.4) and embedded in paraffin wax. Each block of PAT was cut into 7 μm sections and stained with haematoxylin and eosin. Sections were scanned using a NanoZoomer digital slide scanner (Hamamatsu Photonics, Welwyn, UK) to create digital images for analysis. All stereological measurements were performed and analysed blind to the treatment group. The percentage volumes of UL and ML adipocytes were determined using NewCAST stereological software (Visiopharm, Hoersholm, Denmark). A point-counting grid of 25 points was applied over the adipose

sections and meander sampling was used to analyse the adipocyte types. A total of 40 counting frames were used per slide to provide at least 200 points per animal. Unilocular cells were defined as an adipocyte with a diameter larger than 60 µm, after shrinkage. Unilocular cell size was determined by measuring the perimeter of 60-80 of the largest UL adipocytes using the stereology software NDP.view (Hamamatsu Photonics). Tissue shrinkage was estimated by measurement of the diameter of red blood cells in each section and the perimeter measurements of each fetus were adjusted by 40-50% (46). There was no significant difference in tissue shrinkage between the samples from the TX and sham groups.

RNA-sequencing and bioinformatic analysis

Total RNA was extracted from fetal PAT samples using the RNeasy Lipid Tissue Mini Kit (Qiagen, Manchester, UK) and cDNA libraries were prepared in samples with RIN>6 (Agilent bioanalyser 2100 system, Agilent Technologies TDA UK Limited, Stockport, UK). Briefly, mRNA was enriched from total RNA before reverse transcription, and adenylation and barcode ligation was performed after the synthesis of double stranded cDNA. Ligated libraries were enriched with a limited amplification. Indexed libraries were normalised, pooled and sequenced on the Illumina HiSeq 4000 platform, single-end reads (SE50) at the Genomics Core Facility, Cancer Research UK Cambridge Institute, Cambridge, UK.

For each library, original reads files were quantified, trimmed and aligned to the Oar_v3.1 reference genome using Cluster-Flow pipeline tool (version v0.5 dev, fastqc_star pipeline; 47), including the following built-in software: fastqc (version 0. 11.5; 48), trim_galore (version 0.4.2; 49), fastq_screen (version 0.9.3; 50), multiqc (version 0.9dev; 51) and reads alignment software STAR (version 2.5.1b_modified; 52). Mapped reads were sorted and indexed with samtools (53). Since the RNA-seq data were used for gene expression quantification, duplicated reads were kept. Subread software (version 1.5.0-p2; 54) with the function featureCounts was applied to the indexed bam files to count the mapped reads/fragments per annotated gene from the annotation file provided for the sheep genome (Oar_v3.1) release.

Initial quality control included PCA and data from two fetuses were removed as outliers before further analysis. Differentially expressed genes were identified using R (version 3.5.3) DESeq2 package (version 1.22.2; 55), using variance stabilizing transformed expression for counts. Genes with more than one read across all samples within a contrast were retained. Additional filtering of genes with low mean read counts was automatically applied by DESeq2. For each contrast, differentially expressed genes with BH-adjusted P-values < 0.05 were identified. Log2 fold change in gene expression was plotted against the mean of read counts normalized by library size for each gene in MA plots. Different contrasts significant expressed genes were plotted in volcano plots and the summary intersection number of different expressed genes were plotted using UpSetR (version 1.4.0). For heatmap analysis, gene-level transcripts expression values were derived by normalised transformed values estimated by DESeq2.

A Bayesian method implemented in DESeq2 was used to moderate the log2 fold changes obtained for genes with low or variable expression levels. Upregulated and downregulated genes in different contrasts (BH-adjusted p < 0.01 and absolute log2 fold change > 1) were analysed for gene ontology (GO) term enrichment. Gene sets were analysed for over-representation of BP (biological process) and KEGG pathway using R package clusterProfiler (version 3.10.1). Significantly enriched terms were identified by applying the default clusterProfiler algorithm coupled with the Fisher's exact test statistic ($P \leq 0.05$, $q \leq 0.05$). Gene ontology plots were drawn using R packages enrichplot (version 1.2.0) and GOplot (version 1.0.2). Read counts were used in the statistical analysis of mRNA abundance of key genes.

Western blotting

Frozen samples of fetal PAT were homogenised in cold lysis buffer (100 mg/ml; 20 mM sodium orthovanadate, 10 mM β-glycerol phosphate, 50 mM sodium fluoride and protease inhibitor cocktail (Roche, Burgess Hill, UK)) in Lysing Matrix-D tubes using a Super FastPrep 1 homogeniser (MP Biomedicals, Loughborough, UK). Samples were centrifuged at 15000 g for 10 minutes at 4 °C. Extracted protein concentration was measured by a bicinchoninc acid protein assay (Sigma, Poole, UK). Prior to loading, samples were mixed with NuPage 4 x lithium dodecyl sulphate (LDS) loading buffer (2% LDS, 141 mM Tris base, 10% glycerol, 0.51 mM EDTA, 0.22 mM Blue G, 0.175 mM Phenol Red; Life Technologies, Loughborough, UK) and 100 mM DL-dithiothreitol, and heated to 70 °C for 10 minutes (with the exception of those for pS6K quantification, which were heated to 99 °C for 5 minutes). Equal amounts (100 µg) of sample protein were separated using 7.5 % Mini-PROTEAN pre-cast gels (Biorad, Hemel Hempstead, UK) for 50 minutes at 150 V and transferred for 10 minutes at 11 V onto a polyvinylidene difluoride membrane (Immobilon P 0.45 µm, Millipore, Sigma) using the Pierce G2 Fast Blotter (Thermo Scientific, Loughborough, UK). The membrane was incubated with 2.5 % non-fat milk (or bovine serum albumin for phosphorylated proteins) in Tris-buffered saline with 0.1 % Tween-20 for 1 hour at room temperature, followed by incubation overnight at 4 °C with primary antibodies: rabbit polyclonal anti-INSR-β (10 µg/ml, Santa Cruz Biotechnologies, Heidelberg, Germany), rabbit polyclonal anti-IGF-1Rβ (10 µg/ml, Santa Cruz Biotechnologies), rabbit polyclonal anti-leptin receptor (1 µg/ml, Biorbyt, Cambridge, UK), rabbit polyclonal anti-pAkt (1:800, Ser473, Cell Signalling Technology, Hitchin, UK), mouse monoclonal anti-Akt1 (1:1000, Cell Signalling Technology), rabbit monoclonal anti-Akt2 (1:1000, Cell Signalling Technology), rabbit polyclonal anti-pmTOR (1:800, Ser 2448, Cell Signalling Technology), rabbit polyclonal anti-pS6K (1:1000, Thr 389, Cell Signalling Technology), rabbit polyclonal anti-GLUT4 (2.5 µg/ml, Abcam, Cambridge, UK), mouse monoclonal anti-PCNA (2 mg/L, Dako, Cambridge UK), rabbit polyclonal anti-PPARγ (4 µg/ml, Biorbyt) and rabbit polyclonal anti-UCP1 (1:500, Abcam). Each membrane was incubated with a horseradish peroxidase-conjugated anti-rabbit or anti-mouse secondary antibody (GE Healthcare, Amersham, UK) for 1 hour at room temperature. Protein expression was visualised by addition of Clarity Western ECL chemiluminescence substrate (Biorad, Hemel Hempstead, UK) and quantified using Image Lab software (ChemiDoc, Biorad) after normalisation to Ponceau S staining (56). All data were normalised to a quality control sample across all gels and expressed as fold changes, relative to the sham group at 129 dGA, in arbitrary units.

Citrate synthase activity

Citrate synthase activity was measured in homogenised PAT samples by a spectrophotometric enzyme assay. The assay buffer (pH8) contained 0.1 mM 5,5'-dithio-bis-2-nitrobenzoic acid, 1 mM oxaloacetate and 0.3 mM acetyl-CoA. Adipose CS activity was determined from the maximum rate of change of absorbance at 412 nm and 37 °C (rate of thionitrobenzoic acid production) over 3 minute periods, and was expressed as µmoles per minute per mg protein, measured by a bicinchoninc acid protein assay.

Statistical methods

Data were analysed by three-way ANOVA with treatment, gestational age and sex of the fetus as factors (SigmaStat 3.5, Systat Software, San Jose, California, USA). The sex of the fetus had no significant effect on any of the variables measured; data from male and female fetuses were, therefore, combined and analysed by two-way ANOVA followed by the Tukey post-hoc test. Relationships between variables were assessed by linear regression. Significance was regarded as $P<0.05$.

Acknowledgments

The authors would like to thank technical staff at the Department of Physiology, Development and Neuroscience, University of Cambridge for assistance with the experimental animal work, and Margaret Blackberry at the University of Western Australia for the measurement of plasma leptin and IGF concentrations. Sample library preparation and RNA-seq work were performed at the Genomics and Transcriptomics core, which is funded by the UK Medical Research Council (MRC) Metabolic Disease Unit (MRC_MC_UU_12012/5) and a Wellcome Trust Major Award (208363/Z/17/Z). The project was funded in part by the Biotechnology and Biological Sciences Research Council, and a Research Excellence Award from Oxford Brookes University. SEH was supported by a Nigel Groome PhD Studentship, Oxford Brookes University.

1. M. Pope, H. Budge, M.E. Symonds, The developmental transition of ovine adipose tissue through early life. *Acta Physiol.* **210**, 20-30 (2014).
2. M.E. Symonds, M. Pope, H. Budge, The ontogeny of brown adipose tissue. *Annu. Rev. Nutr.* **35**, 295-320 (2015).
3. A.L. Basse, K. Dixen, R. Yadav, M.P. Tygesen, K. Qvortrup, K. Kristiansen, B. Quistorff, R. Gupta, J. Wang, J.B. Hansen, Global gene expression profiling of brown to white adipose tissue transformation in sheep reveals novel transcriptional components linked to adipose remodeling. *BMC Genomics* 16: 215 (2015).
4. A. Mostyn, S. Pearce, H. Budge, M. Elmes, A.J. Forhead, A.L. Fowden, T. Stephenson, M.E. Symonds, Influence of cortisol on adipose tissue development in the fetal sheep during late gestation. *J. Endocrinol.* **176**, 23-30 (2003).
5. D.M. O' Connor, D. Blache, N. Hoggard, E. Brookes, F.B.P. Wooding, A.L. Fowden, A.J. Forhead, Developmental control of plasma leptin and adipose leptin messenger ribonucleic acid in the ovine fetus during late gestation: role of glucocorticoids and thyroid hormones. *Endocrinology* **148**, 3750-3757 (2007).
6. A.J. Forhead, A.L. Fowden, Thyroid hormones in fetal growth and prepartum maturation. *J. Endocrinol.* **221**, 87-103 (2014).
7. S.J. Schermer, J.A. Bird, M.A. Lomax, D.A. Shepherd, M.E. Symonds, Effect of fetal thyroidectomy on brown adipose tissue and thermoregulation in newborn lambs. *Reprod. Fertil. Dev.* **8**, 995-1002 (1996).
8. A.J. Wassner, Congenital hypothyroidism. *Clin. Perinatol.* **45**, 1-18 (2018).
9. J. Léger, E. Ecosse, M. Roussey, J.L. Lanoë, B. Larroque, Subtle health impairment and socioeducational attainment in young adult patients with congenital hypothyroidism diagnosed by neonatal screening: a longitudinal population-based cohort study. *J. Clin. Endocrinol. Metab.* **96**, 1771-1782 (2011).
10. S.Y. Chen, S.J. Lin, S.H. Lin, Y.Y Chou, Early adiposity rebound and obesity in children with congenital hypothyroidism. *Pediatr. Neonatol.* **54**, 107-112 (2013).
11. Y.W. Pan, M.C. Tsai, Y.J. Yang, M.Y. Chen, S.Y. Chen, Y.Y. Chou, The relationship between nonalcoholic fatty liver disease and pediatric congenital hypothyroidism patients. *Kaohsiung J. Med. Sci.* doi: 10.1002/kjm2.12118. (2019).
12. H. Gholami, S. Jeddi, A. Zadeh-Vakili, K. Farrokhfall, F. Rouhollah, M. Zarkesh, M. Ghanbari, A. Ghasemi, Transient congenital hypothyroidism alters gene expression of glucose transporters and impairs glucose sensing apparatus in young and aged offspring rats. *Cell. Physiol. Biochem.* **43**, 2338-2352 (2017).

13. J. Tapia-Martínez, A.P. Torres-Manzo, M. Franco-Colín, M. Pineda-Reynoso, E. Cano-Europa, Maternal thyroid hormone deficiency during gestation and lactation alters metabolic and thyroid programming of the offspring in the adult stage. *Horm. Metab. Res.* **51**, 381-388 (2019).
14. T. Meas, Fetal origins of insulin resistance and the metabolic syndrome: a key role for adipose tissue? *Diabetes Metab.* **36**, 11-20 (2010).
15. B.X. Liu, W. Sun, X.Q. Kong, Perirenal fat: a unique fat pad and potential target for cardiovascular disease. *Angiology* 70, 584-593 (2019).
16. M.J. Obregón, Adipose tissues and thyroid hormones. *Front. Physiol.* **5**, 479 (2014).
17. S.E. Harris, M.J. De Blasio, M.A. Davis, A. Kelly, H.M. Davenport, F.B.P. Wooding, D. Blache, D. Meredith, M. Anderson, A.L. Fowden, S.W. Limesand, A.J. Forhead, Hypothyroidism *in utero* stimulates pancreatic beta cell proliferation and hyperinsulinaemia in the ovine fetus during late gestation. *J. Physiol.* **595**, 3331-3343 (2017).
18. A.L. Fowden, P. Hughes, R.S. Comline, The effects of insulin on the growth rate of the sheep fetus during late gestation. *Q. J. Exp. Physiol.* **74**, 703-714 (1989).
19. B.S. Mühlhäusler, C.L. Adam, E.M. Marrocco, P.A. Findlay, C.T. Roberts, J.R. McFarlane, K.G. Kauter, I.C. McMillen, Impact of glucose infusion on the structural and functional characteristics of adipose tissue and on hypothalamic gene expression for appetite regulatory neuropeptides in the sheep fetus during late gestation. *J. Physiol.* **565**, 185-195 (2005).
20. L.S. Carnevalli, K. Masuda, F. Frigerio, O. Le Bacquer, S.H. Um, V. Gandin, I. Topisirovic, N. Sonenberg, G. Thomas, S.C. Kozma, S6K1 plays a critical role in early adipocyte differentiation. *Dev. Cell* **18**, 763-774 (2010).
21. M.J. Lee, Hormonal regulation of adipogenesis. *Compr. Physiol.* **7**, 1151-1195 (2017).
22. S.H. Um, M. Sticker-Jantscheff, G.C. Chau, K. Vintersten, M. Mueller, Y.G. Gangloff, R.H. Adams, J.F. Spetz, L. Elghazi, P.T. Pfluger, M. Pende, E. Bernal-Mizrachi, A. Tauler, M.H. Tschöp, G. Thomas, S.C. Kozma, S6K1 controls pancreatic β cell size independently of intrauterine growth restriction. *J. Clin. Invest.* **125**, 2736-2747 (2015).
23. S.H. Um, F. Frigerio, M. Watanabe, F. Picard, M. Joaquin, M. Sticker, S. Fumagalli, P.R. Allegrini, S.C. Kozma, J. Auwerx, G. Thomas, Absence of S6K1 protects against age- and diet-induced obesity while enhancing insulin sensitivity. *Nature* **431**, 200-205 (2004).
24. A. Castelló, J.C. Rodríguez-Manzaneque, M. Camps, A. Pérez-Castillo, X. Testar, M. Palacín, A. Santos, A. Zorzano, Perinatal hypothyroidism impairs the normal transition of GLUT4 and GLUT1 glucose transporters from fetal to neonatal levels in heart and brown adipose tissue. Evidence for tissue-specific regulation of GLUT4 expression by thyroid hormone. *J. Biol. Chem.* **269**, 5905-5912 (1994).
25. A.J. Forhead, J. Li, J.C. Saunders, M.J. Dauncey, R.S. Gilmour, A.L. Fowden, Control of ovine hepatic growth hormone receptor and insulin-like growth factor I by thyroid hormones *in utero*. *Am. J. Physiol.* **278**, E1166-1174 (2000).
26. A.J. Forhead, J. Li, R.S. Gilmour, M.J. Dauncey, A.L. Fowden, Thyroid hormones and the mRNA of the GH receptor and IGFs in skeletal muscle of fetal sheep. *Am. J. Physiol.* **282**, E80-E86 (2002).
27. S.U. Devaskar, R. Anthony, W. Hay, Ontogeny and insulin regulation of fetal ovine white adipose tissue leptin expression. *Am. J. Physiol.* **282**, R431-R438 (2002).
28. C. Menendez, R. Baldelli, J.P. Camiña, B. Escudero, R. Peino, C. Dieguez, F.F. Casanueva, TSH stimulates leptin secretion by a direct effect on adipocytes. *J. Endocrinol.* **176**, 7-12 (2003).
29. M.J. Obregón, R. Calvo, A. Hernández, F. Escobar del Rey, G. Morreale de Escobar, Regulation of uncoupling protein messenger ribonucleic acid and 5'-deiodinase activity by thyroid hormones in fetal brown adipose tissue. *Endocrinology* **137**, 4721-4729 (1996).
30. C. Guerra, C. Roncero, A. Porras, M. Fernández, M. Benito, Triiodothyronine induces the transcription of the uncoupling protein gene and stabilizes its mRNA in fetal rat brown adipocyte primary cultures. *J. Biol. Chem.* **271**, 2076-2081 (1996).
31. F. Villarroya, M. Peyrou, M. Giralt, Transcriptional regulation of the uncoupling protein-1 gene. *Biochimie* **134**, 86-92 (2017).
32. D.W. Walker, J.A. Schuijers, Effect of thyroidectomy on cardiovascular responses to hypoxia and tyramine infusion in fetal sheep. *J. Dev. Physiol.* **12**, 337-345 (1989).
33. A.H. Klein, A. Reviczky, J.F. Padbury, Thyroid hormones augment catecholamine-stimulated brown adipose tissue thermogenesis in the ovine fetus. *Endocrinology* **114**, 1065-1069 (1984).
34. S.Y. Wu, M.L. Merryfield, D.H. Polk, D.A. Fisher, Two pathways for thyroxine 5'-monodeiodination in brown adipose tissue in fetal sheep: ontogenesis and divergent responses to hypothyroidism and 3,5,3'-triiodothyronine replacement. *Endocrinology* **126**, 1950-1958 (1990).
35. A.J. Forhead, K. Curtis, E. Kaptein, T.J. Visser, A.L. Fowden, Developmental control of iodothyronine deiodinases by cortisol in the ovine fetus and placenta near term. *Endocrinology* **147**, 5988-5994 (2006).
36. D.H. Polk, S.Y. Wu, C. Wright, A.L. Reviczky, D.A. Fisher, Ontogeny of thyroid hormone effect on tissue 5'-monodeiodinase activity in fetal sheep. *Am. J. Physiol.* **254**, E337-E341 (1988).
37. N. Toyoda, A.M. Zavacki, A.L. Maia, J.W. Harney, P.R. Larsen, A novel retinoid X receptor-independent thyroid hormone response element is present in the human type 1 deiodinase gene. *Mol. Cell. Biol.* **15**, 5100-5112 (1995).
38. P.M. Catalano, L. Presley, J. Minium, S. Hauguel-de Mouzon, Fetuses of obese mothers develop insulin resistance in utero. *Diabetes Care* **32**, 1076-1080 (2009).
39. P.M. Catalano, K. Farrell, A. Thomas, L. Huston-Presley, P. Mencin, S.H. de Mouzon, S.B. Amini, Perinatal risk factors for childhood obesity and metabolic dysregulation. *Am. J. Clin. Nutr.* **90**, 1303-1313 (2009).
40. S.C. Wong, S.M. Ng, M. Didi, Children with congenital hypothyroidism are at risk of adult obesity due to early adiposity rebound. *Clin. Endocrinol.* **61**, 441-446 (2004).
41. S. Arenz, U. Nennstiel-Ratzel, M. Wildner, H.G. Dörr, R. von Kries, Intellectual outcome, motor skills and BMI of children with congenital hypothyroidism: a population-based study. *Acta Paediatr.* **97**, 447-450 (2008).
42. V. Aiceles, F.M. Gombar, F.D.S. Cavalcante, C.D.F. Ramos, Congenital hypothyroidism is associated with impairment of the leptin signaling pathway in the hypothalamus in male Wistar animals in adult life. *Horm. Metab. Res.* **51**, 330-335 (2019).
43. P.S. Hopkins, G.D. Thorburn, The effects of foetal thyroidectomy on the development of the ovine foetus. *J. Endocrinol.* **54**, 55-66 (1972).
44. D. Blache, R.L. Tellam, L.M. Chagas, M.A. Blackberry, P.E. Vercoe, G.B. Martin, Level of nutrition affects leptin concentrations in plasma and cerebrospinal fluid in sheep. *J. Endocrinol.* **165**, 625–637 (2000).
45. A.J. Forhead, J.K. Jellyman, K. Gillham, J.W. Ward, D. Blache, A.L. Fowden, Renal growth retardation following angiotensin II type 1 (AT_1) receptor antagonism is associated with increased AT_2 receptor protein in fetal sheep. *J. Endocrinol.* **208**, 137-145 (2011).
46. M.J. Karvonen, The diameter of foetal sheep erythrocytes. *Acta Anat.* **20**, 53-61 (1954).
47. P. Ewels, F. Krueger, M. Käller, S. Andrews, Cluster Flow: A user-friendly bioinformatics workflow tool. Version 2. *F1000Res.* **5**, 2824 (2016).
48. S. Andrews, F. Krueger, A. Degonds-Pichon, L. Biggins, C. Krueger, S. Wingett, FastQC: a quality control tool for high throughput sequence data. Available at: http://www.bioinformatics.babraham.ac.uk/projects/fastqc. (2012).
49. F. Krueger, P. Ewels, Trim Galore: A wrapper tool around Cutadapt and FastQC to consistently apply quality and adapter trimming to FastQ files, with some extra functionality for MspI-digested RRBS-type (Reduced Representation Bisufite-Seq) libraries. Available at: https://www.bioinformatics.babraham.ac.uk/projects/trim_galore/. (2012).
50. S.W. Wingett, S. Andrews, FastQ Screen: A tool for multi-genome mapping and quality control. *F1000Res.* **7**, 1338 (2018).
51. P. Ewels, M. Magnusson, S. Lundin, M. Käller, MultiQC: summarize analysis results for multiple tools and samples in a single report. *Bioinformatics* **32**, 3047-3048 (2016).
52. A. Dobin, C.A. Davis, F. Schlesinger, J. Drenkow, C. Zaleski, S. Jha, P. Batut, M. Chaisson, T.R. Gingeras, STAR: ultrafast universal RNA-seq aligner. *Bioinformatics* **29**, 15-21 (2013).
53. H. Li, B. Handsaker, A. Wysoker, T. Fennell, J. Ruan, N. Homer, G. Marth, G. Abecasis, R. Durbin, 1000 Genome Project Data Processing Subgroup, The Sequence Alignment/Map format and SAMtools. *Bioinformatics* **25**, 2078-2079 (2009).
54. Y. Liao, G.K. Smyth, W. Shi, The Subread aligner: fast, accurate and scalable read mapping by seed-and-vote. *Nucleic Acids Res.* **41**, e108, (2013).
55. The R Foundation, The R Project for Statistical Computing. Available at: https://www.R-project.org/. (2018).
56. I. Romero-Calvo, B. Ocón, P. Martínez-Moya, M.D. Suárez, A. Zarzuelo, O. Martínez-Augustin, F.S. de Medina, Reversible Ponceau staining as a loading control alternative to actin in Western blots. *Anal. Biochem.* **401**, 318-320 (2010).

Please review all the figures in this paginated PDF and check if the figure size is appropriate to allow reading of the text in the figure.

If readability needs to be improved then resize the figure again in 'Figure sizing' interface of Article Sizing Tool.